



WICHITA STATE
UNIVERSITY

UNIVERSITY LIBRARIES

**Design and synthesizing of hemoglobin-
based multifunctional fibers for improved
carbon monoxide absorption rates**

Item Type	Article
Authors	Pham, Anh;Subeshan, Balakrishnan;Asmatulu, Eylem;Asmatulu, Ramazan
Citation	Pham, A., Subeshan, B., Asmatulu, E. et al. Design and Synthesizing of Hemoglobin-Based Multifunctional Fibers for Improved Carbon Monoxide Absorption Rates. <i>BioNanoSci.</i> 15, 184 (2025). https://doi.org/10.1007/s12668-025-01807-8
DOI	10.1007/s12668-025-01807-8
Publisher	Springer
Download date	2026-06-18 16:58:52
Link to Item	https://hdl.handle.net/10057/29157



Design and Synthesizing of Hemoglobin-Based Multifunctional Fibers for Improved Carbon Monoxide Absorption Rates

Anh Pham¹ · Balakrishnan Subeshan¹ · Eylem Asmatulu¹ · Ramazan Asmatulu¹

Accepted: 7 January 2025 / Published online: 14 January 2025

This is a U.S. Government work and not under copyright protection in the US; foreign copyright protection may apply 2025

Abstract

This study is aimed at developing advanced materials for carbon monoxide (CO) capture by producing hemoglobin (Hb)-based electrospun multifunctional micro- and nanofibers blended with polyvinylpyrrolidone (PVP). Unlike conventional CO trapping materials such as activated carbon, ammoniacal cuprous chloride, zeolites, and metal-organic frameworks (MOFs), Hb/PVP fibers leverage the simplicity and scalability of electrospinning to produce continuous, defect-free flexible fibers with tunable micron- to nanoscale diameters. The process enables precise control over fiber morphology, surface area, porosity, and hydrophilicity, providing significant advantages for optimizing CO adsorption rates. Moreover, the inclusion of Hb introduces a biomimetic advantage through its intrinsic CO-binding affinity, offering higher specificity and interaction potential compared to traditional physical adsorption or chemical frameworks. Experimental results revealed that fibers with 8 wt.% PVP exhibited the smallest and most uniform diameters, while higher PVP concentrations (16, 32 wt.%) enhanced hydrophilicity, with complete water absorption occurring within 400 and 200 seconds, respectively. Structural and compositional analyses using confocal laser scanning microscopy (CLSM) and Fourier transform infrared spectroscopy (FTIR) confirmed the integrity and chemical characteristics of the fibers. Thermogravimetric analysis (TGA) and differential scanning calorimetry (DSC) established their thermal stability, with critical transitions at approximately 80 °C (denaturation) and 200 °C (decomposition). Degradation was observed between 200 and 430 °C, corresponding to significant weight loss. These findings demonstrate the potential of Hb/PVP fibers as exceptional alternatives for CO capture. This study may open new possibilities for increasing the absorption rate of highly porous fibers for toxic CO capture in the bloodstream and address other related concerns.

Keywords Electrospinning · CO absorption · Multifunction fibers · Hemoglobin · Testing · Characterizations

1 Introduction

1.1 General Background

Carbon monoxide (CO) adversely affects human health, the products of some industrial processes, and the environment. Inhalation of CO can lead to acute poisoning, with symptoms ranging from fatigue, headache, and nausea to coma and potentially death, depending on the concentration of CO in the bloodstream [1]. Survivors of severe poisoning often experience enduring neurological damage, including cognitive deficits, speech impairment, depression, and symptoms

resembling Parkinson's disease [2]. Moreover, chronic exposure harms cardiovascular health and cognition [3]. Beyond health impacts, CO contamination disrupts industrial processes by compromising product quality [4], while its oxidation contributes to greenhouse gas emissions in the form of carbon dioxide. Given these varied risks, effective CO capture and removal are critical for mitigating its detrimental effects. Materials like activated carbon, ammoniacal cuprous chloride, zeolite, and metal-organic frameworks (MOFs) are widely used for CO capture [5]. However, these materials often face limitations such as high production costs, limited reusability, and insufficient performance in dynamic environments. In recent years, electrospun nanofibers, one class of nanomaterials, have emerged as promising candidates for CO capturing, offering advantages such as large surface area, tailored properties, enhanced reactivity,

✉ Ramazan Asmatulu
ramazan.asmatulu@wichita.edu

¹ Department of Mechanical Engineering, Wichita State University, 1845 Fairmount Street, Wichita, KS 67260, USA

and multifunctionality under physiological conditions, making them particularly effective in biomedical and industrial applications [6, 7].

Electrospinning is a versatile and efficient technique with considerable potential for capturing toxic gases, particularly CO. This method involves generating continuous nanofibers from various polymers by applying a high voltage to a polymer solution. When the electrical field generated by the voltage source exceeds the critical surface tension of the liquid, a droplet forms at the tip of the needle and deforms to create the “Taylor cone” [8]. Subsequently, a charged jet emerges and is directed toward a collector. During this process, the jet undergoes stretching, and the solvent evaporates, resulting in the formation of ultrafine fibers. These fibers with diameters, typically ranging from tens to hundreds of nanometers, exhibit a high surface area-to-volume ratio, porosity, and a low weight-to-volume ratio [9–11]. These properties make them highly suitable for gas adsorption applications, such as CO capture. To enhance their performance, these fibers often incorporate advanced materials that optimize permeability and adsorption selectivity. MOFs have gained particular attention due to their tunable pore structures, high surface areas, and strong gas affinity. Recent developments in MOF-functionalized fibers have demonstrated significant improvements in both adsorption capacity and selectivity [12–15].

Electrospinning’s effectiveness in capturing gases depends on various factors, mainly related to the properties of the polymer solution and how the process parameters are carried out. Polymer solution properties, such as concentration, viscosity, molecular weight, and solvent type, play a pivotal role in determining the characteristics of the resultant nanofibers. For instance, variations in polymer concentration can impact fiber diameter, while changes in viscosity affect the jet stability and the eventual fiber morphology [16]. Simultaneously, process variables during electrospinning, including applied voltage, distance between the spinneret and collector, and flow rate of the polymer solution, exert significant influence on the electrospun nanofiber properties. Voltage regulates jet initiation and trajectory, whereas the distance between the spinneret and collector controls fiber alignment and stretching.

Additionally, the flow rate influences the deposition rate and uniformity of the fibers [17–22]. External factors such as ambient temperature, viscosity, humidity, and the geometry of the spinneret and collector further impact the final fiber properties. Optimization of the parameters is critical for achieving nanofibers tailored to specific gas adsorption requirements. Through parameter tuning, researchers can enhance fiber selectivity, durability, and adsorption efficiency, addressing challenges in CO capture. Electrospun nanofibers have gained attention not only as adsorbents but also as catalytic supports for CO conversion into less toxic gases like carbon dioxide [23–26]. Catalysts such as

platinum and palladium supported on nanofibers exhibit high catalytic efficiency. However, their general application is constrained by the high cost of noble metals. Alternative approaches, such as the use of polymeric nanofibers, have shown potential in reducing reliance on expensive materials. Sargazi et al. [27] developed an electrospun nanofibrous membrane from polyvinyl alcohol (PVA)/chitosan (CS) for CO adsorption, surpassing the capacity of activated carbon, zeolite, and MOF. Through multi-objective optimization, their PVA/CS adsorbent achieved a desirability value of 0.953, marking a new era in nanofiber design for CO capture.

The structure of Hb is unique among proteins. Hb is a globular protein composed of four subunits, each containing a heme group with an iron atom at its center. These subunits come together to form a quaternary structure, giving Hb its distinctive shape and functional properties, enabling it to bind and transport oxygen and carbon dioxide in the bloodstream. The unique structure of Hb, particularly its ability to bind to gases, can inspire the development of materials for effectively absorbing CO. Electrospinning has been successfully used to incorporate Hb into nanofibrous materials. For instance, Ravichandran et al. [28] successfully generated hemoglobin/gelatin/fibrinogen (Hb/gel/fib) nanofibers using electrospinning technology. Sahtani et al. [29] also present a method where Hb-assisted carbon nanofibers are prepared through electrospinning. Another study reported the effectiveness of adding copolymers and other additives to produce continuous, uniform, and smaller-diameter Hb nanofibers. By introducing carbon nanotubes (CNT) and collagen to enhance conductivity and reduce viscosity in the Hb solution, they achieved bead-free, uniform, and smooth Hb/CNT/collagen fibers. These studies highlight the versatility of electrospinning in creating Hb-based nanofibers for various applications. In the context of biosensors, Wu et al. [30] present a novel hydrogen peroxide biosensor based on Hb combined with electrospinning composite nanofibers. Collectively, these findings highlight the adaptability of both electrospinning and different material compositions in facilitating the production of Hb nanofibers, offering opportunities for innovative applications such as CO capturing.

Poly(vinylpyrrolidone) (PVP) plays a pivotal role in enhancing the processability and flexibility of Hb in electrospinning, owing to its remarkable versatility and solubility in electrospinning applications [31]. In this context, PVP acts as a carrier polymer for Hb, enhancing the processability of Hb, ensuring the successful fabrication of multifunctional electrospun fibers, and promoting the CO absorption abilities in the blood circulation because of its hydrophilic nature, molecular interaction, non-toxic, pH-stable, enhanced processability, controlled degradation, biocompatible, and biodegradable features. These capabilities find significance in their previous applications, where PVP has been instrumental in improving

the spinnability of conjugated polymers, as evidenced in the manufacturing of stretchable organic electrochemical transistors [32]. Medical applications such as wound dressings, scaffolds, biosensors, biomaterials, and biopolymers have been successfully electrospun into nanofibers with the addition of PVP to the polymeric solution. The solubility and compatibility of PVP make it a valuable component in various composite systems. For example, PVP has been combined with CS to produce composite fibers through electrospinning, demonstrating its versatility in generating innovative materials [33]. Additionally, PVP has been utilized in the fabrication of composite nanofibers with AgCl through electrospinning, indicating its potential in creating functional materials in biomedical fields [34]. These studies highlight the crucial role of PVP in facilitating the production of electrospun fibers, including those containing hemoglobin and other supporting materials.

Notably, the use of PVP in Hb electrospinning for CO capturing represents a novel approach, highlighting its unexploited potential for advancing protein-based fiber systems. This study marks the first successful fabrication of Hb-based multifunctional micro- and nanofibers blended with PVP using electrospinning. Various concentrations of PVP (0, 4, 8, 16, and 32 wt.%) with respect to Hb were incorporated to achieve continuous, uniform micro- and nanofibers with diameters in the micro or nanoscale range. The main focus of the study is to analyze Hb/PVP fiber properties, including morphology, chemical composition, thermal behavior, and wettability. These findings highlight the potential use of Hb/PVP fibers as effective CO adsorbents in biomedical and environmental applications, paving the way for further optimization and application in various settings.

1.2 Binding Mechanism of Hemoglobin to Carbon Monoxide

Hb, the structure of which is shown in Fig. 1, is a complex protein consisting of four subunits, each containing a heme group with an iron (Fe^{2+}) ion at its center. These heme groups are responsible for binding oxygen molecules during respiration. However, Hb can also bind to other ligands, such as CO, forming a stable complex known as carboxyhemoglobin. CO binds to Hb with an affinity that is 250 times higher than that of oxygen. This interaction significantly affects the equilibrium between oxygenated and deoxygenated states of Hb, illustrating the remarkable specificity and strength of CO binding to Hb [35, 36].

CO forms bonds with transition metals (e.g., Fe, Cu, Co, Ni, Cr, Mn) through a mechanism known as synergistic π^* back-bonding (Fig. 2a), consisting of three main components, resulting in the formation of a partial triple bond. The first component of the bond formation is a σ bond, which emerges from the synergistic interaction of ligand-to-metal σ donation, involving the 3σ molecular orbital of CO (Fig. 2b) and a suitable atomic orbital on the metal atom [38], with the overlap of the nonbonding or weakly anti-bonding sp-hybridized electron pair on carbon and a blend of d-, s-, and p-orbitals on the metal. The second component involves two π bonds that are formed from the overlap of filled d-orbitals on the metal with a pair of antibonding π^* orbitals (π_x^* and π_y^*) projecting from the carbon atom of the CO molecule [5]. For this π bonding to occur, the transition metal must have available d-electrons and be in a relatively low oxidation state (0 or +1), favoring the back-donation of electron density. As electrons from the metal fill the π -antibonding orbital of CO, they weaken the carbon-oxygen bond compared to free carbon monoxide while simultaneously strengthening

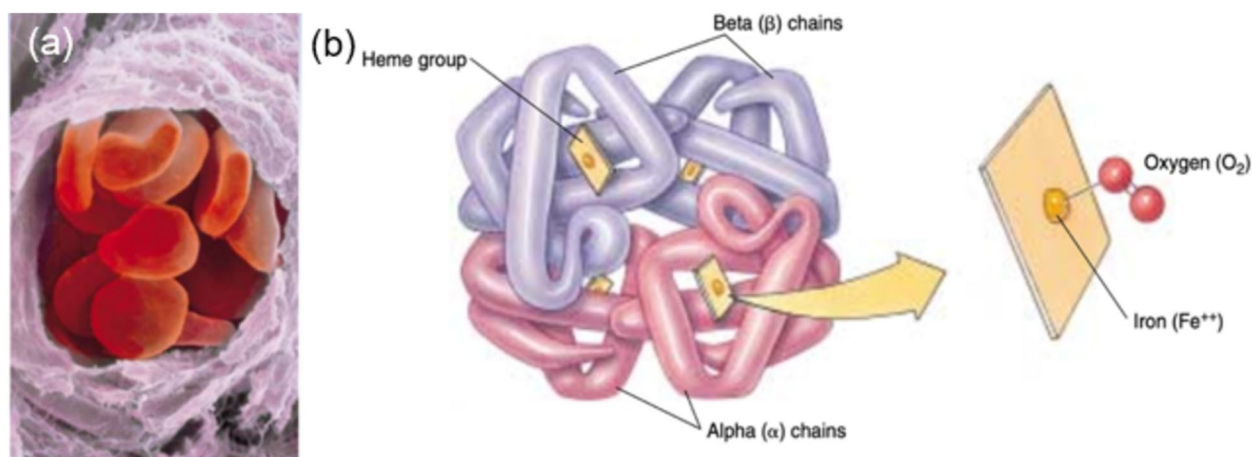


Fig. 1 **a** SEM of red blood cells in a ruptured blood vessel, **(b)** Structure of hemoglobin [37]

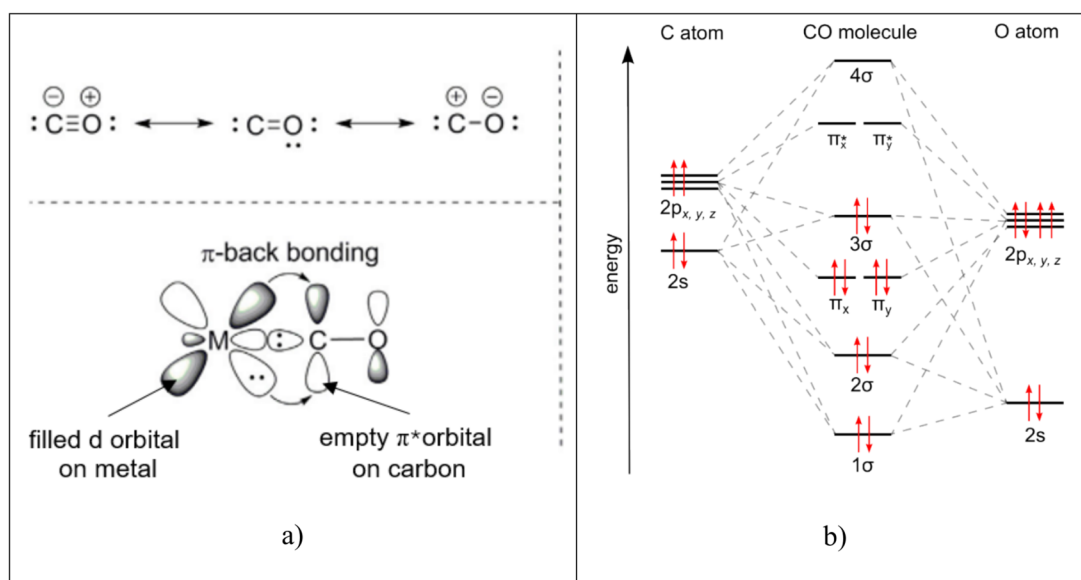


Fig. 2 Images show (a) bonding of CO with transition metals and (b) ligand-to-metal donation and molecular orbital of CO [38]

the metal-carbon bond. This mechanism explains the high affinity of CO for transition metals in low oxidation states and its ability to form stable complexes, such as those seen in the binding of CO to the Fe^{2+} in the Hb group.

The structure of Hb is uniquely adapted to facilitate the binding of CO within the heme pocket, and the iron atom can undergo conformational changes upon CO binding, which helps orient the iron atom towards the plane of the porphyrin ring, facilitating the binding process. This movement of the iron atom disrupts the geometry of the heme group, making it conducive for interactions with CO [39]. Additionally, specific amino acid residues within Hb, such as the distal histidine, contribute to the protein's affinity for CO by inhibiting steric hindrance and making the binding site more accessible [40].

Furthermore, the structural arrangement of the heme pocket and surrounding amino acids play crucial roles in enhancing CO binding affinity to the other structures. Studies have shown that the binding of CO to Hb induces specific structural changes in the protein, including alterations in heme-heme interactions and the orientation of the distal side of the heme group. These structural modifications enhance the affinity and stability of the complex structures, making the hemoglobin structure well-suited for CO capturing [41]. The novelty of this work is that for the first time, Hb-based multifunctional micro- and nanofibers were produced using electrospinning materials, and their characteristics were determined using various techniques. It is believed that this approach can accelerate the CO absorption rate of these flexible multifunctional micro- and nanofibers in the bloodstream.

2 Experiment

2.1 Materials

Bovine Hb powder (64.5 kDa) was purchased from Thermo Fisher Scientific. PVP and 2,2,2-Trifluoroethanol (TFE) (99%) were purchased from Sigma-Aldrich. No further modification or purification was conducted on these materials prior to the experimental use.

2.2 Preparation of Hemoglobin-Based Electrospun Fibers

To fabricate pristine Hb fibers (Hb-0), 11 wt.% of Hb was added into TFE solution (or 175 mg/mL Hb/TFE) [42]. For the generation of Hb/PVP-4, -8, -16, and -32 samples, 4, 8, 16, and 32 wt.% of PVP (with respect to Hb) were dissolved in TFE, respectively. The Hb powder was then added to the homogeneous PVP/TFE mixtures afterward. All mixtures were kept stirring at room temperature for 4 hrs. Hb-based fibers with different concentrations of PVP were obtained by electrospinning process (Fig. 3). The prepared solution was transferred to a 10-ml syringe and fixed on a syringe pump. High voltage supplies were used to apply 17 kV at the attached 22-gauge needle and -5 kV at the collector. The distance between the needle tip and the collector was 20 cm. Taylor cone could be observed in the fibers that were collected on the aluminum foil (Fig. 4).

Fig. 3 Schematic diagram of the electrospinning process used in this study

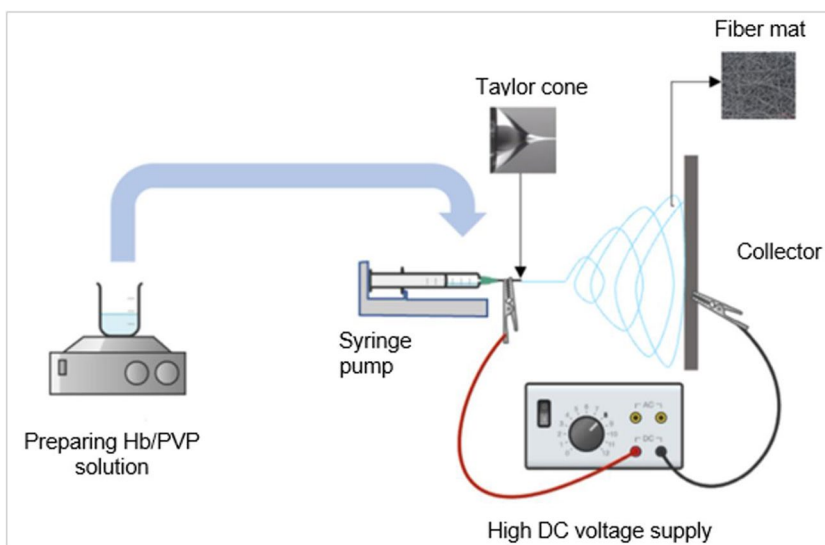


Fig. 4 Taylor cone formation of Hb/PVP solution during electrospinning process and Hb/PVP fiber generation

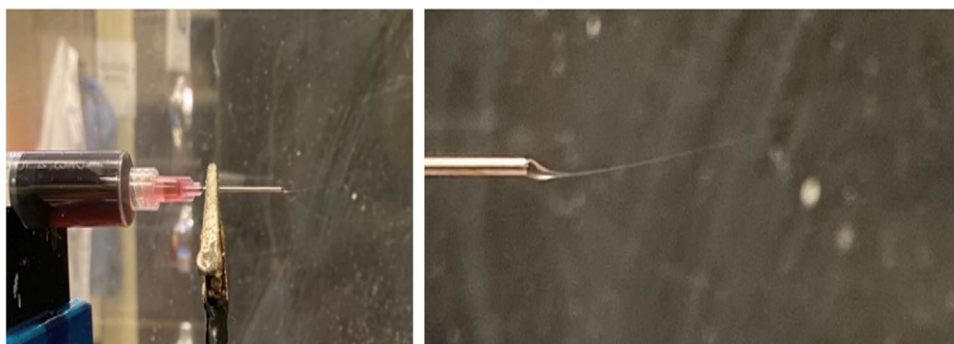


Table 1 Hb-based electrospun fiber samples with different concentrations of PVP

Sample	PVP (wt.% respect to Hb)
Hb-0	0
Hb/PVP-4	4
Hb/PVP-8	8
Hb/PVP-16	16
Hb/PVP-32	32

The sample labels with different concentrations of PVP in the Hb/TFE solution are shown in Table 1.

2.3 Characterizations

Confocal laser scanning microscopic (CLSM) images captured by Keyence VK-X1000 revealed the morphology of Hb-based electrospun fibers with varying concentrations of PVP. Fourier transform infrared spectrophotometry (FTIR) was employed to investigate the composition and chemical characteristics of the composite nanofibers using a Nicolet™ iS50 infrared microscope. The FTIR tests were

conducted with an average of 128 scans, using a resolution of 4 cm⁻¹ and covering a spectral range from 15 to 27,000 cm⁻¹. Thermogravimetric analysis (TGA) was employed using TA Q500 TGA equipment under a nitrogen atmosphere. The temperature range was set from 32 °C to 800 °C, with a heating rate of 10 °C/min. This analysis was used to study the thermal degradation of the samples. Differential scanning calorimetry (DSC) was conducted to investigate the thermal transitions of the fiber samples. DSC experiments were conducted using a Q1000 TA instrument, with temperatures ranging from 0 °C to 220 °C and a heating rate of 10 °C/min. The surface wettability of all samples was assessed using a contact angle goniometer (Model #CAM 100, KSV Instruments Ltd., Helsinki, Finland). WCA tests are typically performed three times for each sample to ensure the accuracy of the data and then averaged to measure the wettability performance of the samples. CLSM, TGA, and DSC were conducted at the National Institute for Aviation Research (NIAR). These comprehensive analytical examinations provide valuable insights into the structural, compositional, thermal, and surface properties of the Hb-based electrospun fibers.

Fig. 5 Optical images of Hb-based fibers (a) without PVP and (b) with 8 wt.% PVP

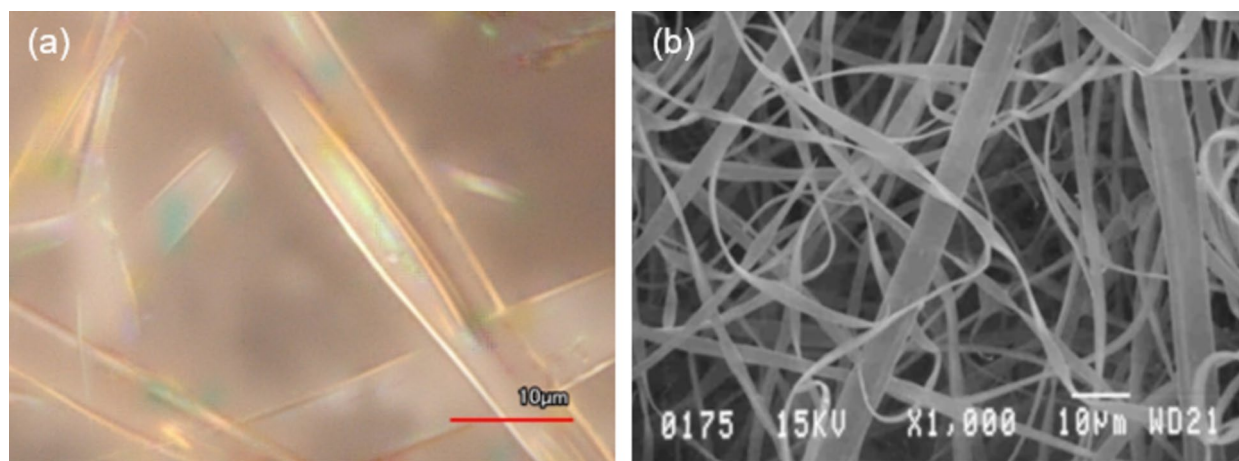
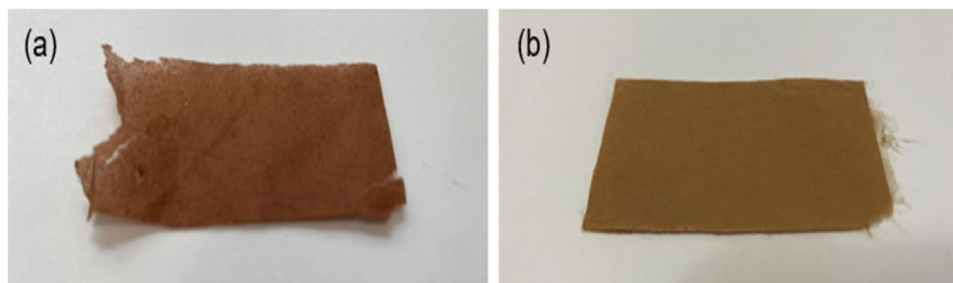


Fig. 6 Micro-belt Hb fibers: a in this study (Hb-0 fiber), and (b) in the Barnes et al. study [42]

3 Results and Discussion

3.1 Morphological Analysis of Fibers

In the present study, the Hb/TFE solution underwent direct formation in the blending PVP through electrospinning. The visible effect of blending PVP in Hb/TFE solution can be observed in Fig. 5. Diverging from the Hb-0 fiber depicted in Fig. 5a, which was characterized by solvent retention on the fibers, displaying a plasticized appearance. The introduction of PVP into the Hb/TFE solution yielded samples exhibiting a more fibrous and uniform texture, which is evident in Fig. 5b, illustrating Hb/PVP-8 fibers.

The CLSM image of the Hb-0 fiber depicted in Fig. 6a confirms the micro-belt (ribbon-like) shape of the Hb fibers, as demonstrated in the work of Barnes et al. [42] (Fig. 6b). Upon analyzing Fig. 6a, the fiber diameter of the Hb fiber is measured to be approximately $5.56 \pm 1.75 \mu\text{m}$, which is considered to be relatively large for the fiber fabrication. The large standard deviation also indicates the inconsistency of fiber diameters and distribution within the Hb-0 fiber.

The formation of the ribbon-like structure arises as a consequence of solvent evaporation during the

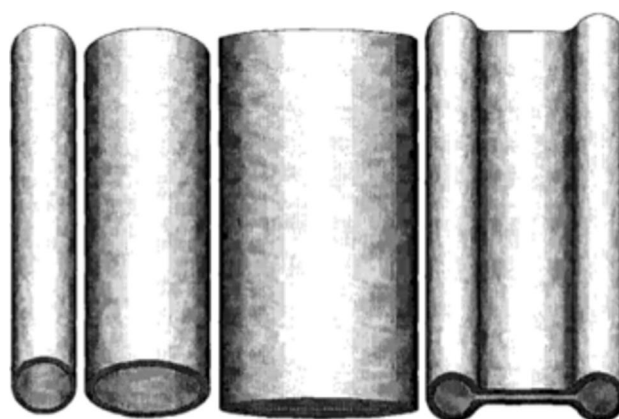


Fig. 7 Mechanism of ribbon-like fiber formation [22]

electrospinning. In instances where solvent retention is elevated within the polymer, which is referred to as wet fibers, these fibers undergo deformation, adopting a flattened morphology as they accumulate on the collector. The mechanism is illustrated in Fig. 7, where it is suggested that a polymer skin forms around the liquid core as the solvent evaporates from the surface of the jet. Subsequently, under ambient pressure, solvent evaporation from the core

causes the circular cross-sectional liquid core to deform into an elliptical shape, which then flattens over time as the fibers reach the collector [43].

Although Hb was fabricated into fibers, the resulting structures exhibited discontinuity, appearing ruptured internally. This behavior is attributed to the globular structure of Hb as a protein, which lacks sufficient chain entanglements and exhibits low viscosity in aqueous solutions [44, 45]. As a result, electrospinning proteins present a significant challenge. However, the incorporation of PVP into the Hb/TFE solution enabled the formation of continuous micron and nanoscale fibers. PVP was selected for its advantageous properties. Firstly, PVP is well-established as a reliable polymer for electrospinning, offering a straightforward process and serving as an effective fibrous matrix. Secondly, its water solubility and hydrophilicity make it a widely used polymer in diverse applications. The specific parameters of the Hb and PVP solutions during electrospinning influence fiber formation and their resulting properties, including

morphology, diameter, porosity, and functionality. Among these parameters, polymer concentration plays a critical role, as it directly impacts solution viscosity, jet stability, and fiber formation. At lower PVP concentrations, such as 4 wt.%, reduced viscosity leads to insufficient chain entanglement, resulting in bead formation and irregular fiber diameters, as observed in the CLSM images. These images, presented in Fig. 8, highlight the influence of PVP on the morphology of Hb-0 fibers. The addition of PVP mitigated the ribbon-like structures observed in Hb-0 fibers, enabling the formation of circular fibers with significantly reduced diameters compared to Hb-0 fibers shown in Fig. 6a. The results demonstrate that increasing PVP concentration enhances chain entanglement in the Hb/PVP solution, leading to the development of continuous, uniform, bead-free electrospun fibers under ambient conditions, which may be useful for improved CO absorption rates in the blood [46].

The diameter of electrospun fibers is a critical factor influencing gas diffusion and adsorption properties, as it

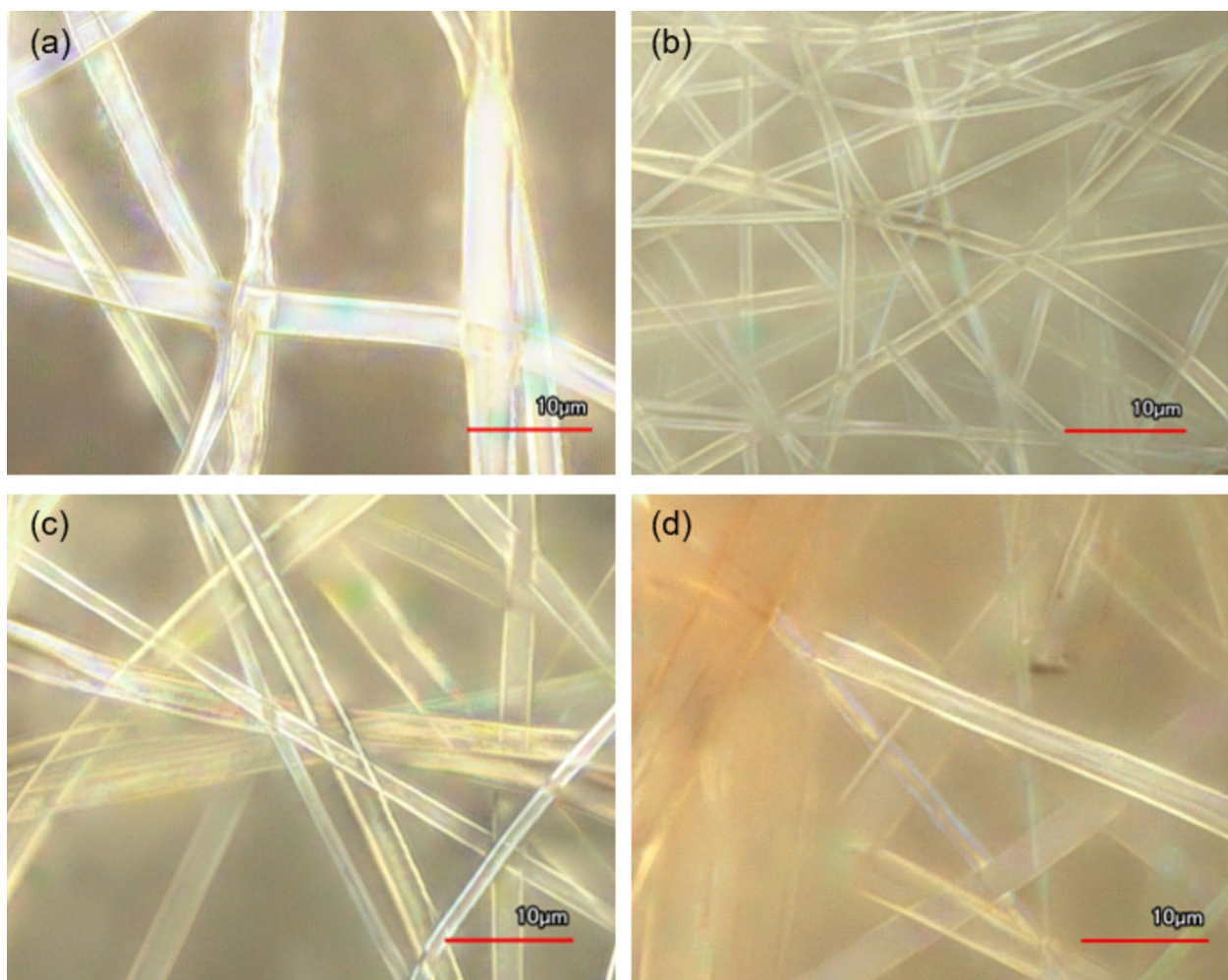


Fig. 8 CLSM images of (a) Hb/PVP-4, (b) Hb/PVP-8, (c) Hb/PVP-16, and (d) Hb/PVP-32 fibers

directly affects surface area, porosity, and structural uniformity. In this study, the addition of PVP at 8 wt.% in the Hb/TFE solution produced fibers with a consistent diameter of approximately $0.90 \pm 0.27 \mu\text{m}$, compared to the larger, irregular diameters observed in samples without PVP or at higher PVP concentrations. These fibers are in the form of micro- and nanoscale ranges. CLSM images (Fig. 8b) reveal the uniform size and distribution of the fibers. Furthermore, Hb/PVP-8 fibers exhibited interconnected interior porosity (usually between 48% and 65%), likely resulting from thermally induced phase separation during solvent evaporation [47]. These uniform and flexible fibers also showed enhanced porosity and surface area (usually between $200 \text{ m}^2/\text{g}$ and $450 \text{ m}^2/\text{g}$), which likely contributes to improved diffusion pathways for CO.

The specific surface area and pore size of Hb/PVP fibers are critical factors influencing their performance in CO adsorption. Smaller fiber diameters, as observed in the Hb/PVP-8 samples, are directly correlated with increased specific surface area, providing more active sites for gas adsorption. These submicron fibers (diameter $\sim 0.90 \pm 0.27 \mu\text{m}$) significantly enhance adsorption efficiency by maximizing the interaction interface between CO molecules and the fiber matrix. In contrast, the larger diameters observed in Hb-0, and Hb/PVP-32 fibers reduce the effective surface area, thereby limiting their adsorption capacity. Pore size further impacts CO adsorption by influencing accessibility to the fiber interior and the strength of intermolecular interactions. Micropores within the Hb/PVP-8 fibers offer a high surface area-to-volume ratio, enhancing the confinement effect and promoting stronger van der Waals forces. This confinement amplifies molecular interactions, increasing adsorption energy and rendering these fibers highly effective for CO capture.

Conversely, the ribbon-like morphology and larger diameters observed in Hb-0 fibers are associated with solvent retention and inconsistent fiber formation, leading to reduced porosity and less effective gas interaction. The non-linear relationship between PVP concentration and fiber diameter, as seen in the Hb/PVP-4, -16, and -32 samples, suggests that factors such as chain entanglement, viscosity, and jet instability during electrospinning significantly influence fiber morphology. For instance, larger diameters in some samples may result in reduced porosity, limiting gas diffusion efficiency, while excessive porosity in others might compromise the structural integrity required for consistent adsorption performance. The porous structures observed in Hb/PVP-8 fibers, attributed to thermally induced phase separation, are particularly advantageous for gas adsorption applications. These pores increase the accessible surface area, providing more binding sites for CO molecules and enhancing the overall adsorption capacity.

The biomimetic properties of Hb enhance the fibers' CO adsorption efficiency. The heme group in Hb exhibits a strong natural affinity for CO through the coordination bond formed between the iron atom and the CO molecule. This specific and selective interaction enables effective CO binding, outperforming conventional adsorption mechanisms that rely solely on physical forces. Furthermore, the incorporation of PVP into the fiber matrix enhances hydrophilicity, ensuring efficient performance in aqueous environments by maintaining the accessibility and integrity of active sites. This synergistic combination of Hb's intrinsic CO-binding capability and PVP's structural support optimizes the overall adsorption process. Intermolecular forces also play a pivotal role in adsorption performance. Beyond coordination bonding, van der Waals forces between CO molecules and the fiber surface further stabilize adsorbed molecules, particularly within the confined micropores of Hb/PVP-8 fibers. While less dominant, electrostatic interactions may also contribute to adsorption, particularly under conditions that facilitate charge distribution within the fibers. Together, these forces ensure efficient and selective CO capture, with Hb/PVP-8 fibers exhibiting the highest adsorption potential due to their optimized morphology and structural properties.

From the analysis of Figs. 8a, c, and d, the diameters of Hb/PVP-4, -16, and -32 fibers were measured at approximately 2.87 ± 0.57 , 2.28 ± 0.66 , and $2.74 \pm 1.08 \mu\text{m}$, respectively, predominantly within the micron scale. Interestingly, the average fiber diameters did not display consistent patterns with increasing PVP concentration in Hb fibers. These findings indicate a non-linear correlation between PVP concentration and fiber diameter, potentially caused by structural heterogeneities within the fibers [48]. Such inconsistencies in structure can hinder gas diffusion by creating regions of reduced porosity or uneven fiber surfaces, limiting the accessibility of active sites and impeding the diffusion of gas molecules through the fibrous network.

Surface tension, influenced by solvent composition and PVP content, also played a significant role in determining fiber morphology. High surface tension destabilized the Taylor cone, leading to droplet formation rather than continuous fibers. The addition of PVP effectively reduced the surface tension of the Hb/TFE solution, stabilizing the electrospinning jet and enabling the formation of defect-free fibers. This reduction in surface tension contributed to the smaller fiber diameters observed in Hb/PVP-8 samples, compared to the larger, ribbon-like fibers produced in Hb-0 samples without PVP. Additionally, the electrical conductivity of the solution was enhanced by the presence of Hb, a protein with charged groups. This improved charge density promoted elongation of the polymer jet under the electric field, resulting in finer and more uniform fiber diameters. However, the globular structure of Hb posed challenges, as it lacked sufficient chain entanglement to form robust fibers independently.

The study primarily aimed to develop highly porous (40–60%) and Hb-based multifunctional fibers with PVP for CO adsorption. Porosity values were estimated based on theoretical considerations and qualitative observations of the fiber structures. Porosity of Hb/PVP fibers was inferred by comparing the bulk densities of the polymer components to the approximate apparent density of the fiber network. According to literature, electrospun fibers typically exhibit porosities ranging from 30–80%, depending on factors such as fiber diameter, packing density, and alignment. In this study, the relatively large micron-scale fiber diameters, combined with the visibly loose packing observed in CLSM images (Fig. 8), suggest that the Hb/PVP fibers have a porosity within the 40–60% range. Furthermore, the incorporation of PVP facilitated pore formation by reducing the viscosity and surface tension of the Hb/TFE solution. This reduction promoted phase separation and solvent evaporation during the electrospinning process, naturally introducing void spaces between fibers and supporting the estimated porosity values.

While CLSM provided valuable qualitative insights into fiber morphology, including surface texture, diameter uniformity, and pore distribution, it is limited in its capacity to quantitatively assess porosity. The resolution and depth of field of CLSM are typically insufficient to capture intricate internal pore networks, particularly when pore sizes fall below the resolution threshold or are deeply embedded within the fibrous matrix. Consequently, porosity values derived from CLSM observations remain approximate and should be interpreted cautiously. Higher-resolution techniques, such as scanning electron microscopy (SEM) or gas adsorption methods (e.g., Brunauer–Emmett–Teller (BET) analysis), could offer quantitative data on pore size distribution and porosity. However, these methods were beyond the scope of this study. Despite these limitations, the qualitative observations from CLSM, combined with theoretical considerations, provide meaningful approximations of porosity in the context of this study. The estimated porosity values align with the qualitative evidence of loose packing and visible voids in the fiber mats, suggesting that the interconnected porous structure facilitates gas diffusion.

The relationship between fiber diameter, porosity, and gas diffusion is governed by fundamental principles of mass transfer. In smaller-diameter fibers, reduced diffusion distances and increased surface area enhance the adsorption of gas molecules by providing more accessible pathways for molecular interaction. This effect is particularly evident in Hb/PVP-8 fibers, where the uniform submicron diameter enables efficient diffusion throughout the fibrous matrix. On the other hand, larger diameters, as observed in Hb-0 and Hb/PVP-32 fibers, create diffusion barriers that diminish the rate and capacity of adsorption. Porosity also plays a critical role: interconnected pores reduce tortuosity, facilitating

gas penetration into the fiber interior and maximizing the effective adsorption area. In contrast, dense or irregular fiber structures impede gas transport. The Hb/PVP-8 fibers' optimal combination of submicron diameter, uniform morphology, and interconnected porosity positions them as superior candidates for CO adsorption. Their increased surface area-to-volume ratio enhances CO binding efficiency, while the uniformity in diameter ensures predictable and consistent diffusion kinetics. These properties are particularly advantageous for applications requiring rapid and efficient gas adsorption, such as biomedical devices for CO removal from the bloodstream or environmental systems for CO capture.

The increased presence of PVP contributed to jet instability during the electrospinning process, leading to regions rich in both solvent and polymer on the surface of the Hb/PVP fibers. PVP likely reduced the viscosity and surface tension of the Hb/TFE solution while acting as a polymer carrier or guide during fiber formation. This unique property of PVP has been widely utilized in electrospinning to fabricate fibers from materials that are difficult or impossible to spin. As PVP fully dissolved in the Hb/TFE solution, its unlimited solubility facilitated the manifestation of all solution properties in the resulting fiber structures under ambient conditions [49].

The morphological characteristics of the Hb/PVP fibers synthesized in this study were critically compared with MOF-functionalized electrospun fibers reported in the literature. A few studies highlight that MOF-polymer systems produce fibers with reduced diameters and enhanced porosity. For example, the incorporation of MOFs into polymer matrices reduces fiber diameters and creates hierarchical pore structures. This refinement arises from the uniform dispersion of MOF nanoparticles, which act as nucleation sites during electrospinning, promoting the formation of thinner and more porous fibers. In comparison, the Hb/PVP-8 fibers fabricated in this study exhibit an average diameter of $0.90 \pm 0.27 \mu\text{m}$. Although slightly larger, these fibers achieve significant porosity and uniformity through phase separation and polymer chain entanglement facilitated by PVP. Unlike MOF-functionalized fibers, which depend on nanoparticle distribution for pore formation, the Hb/PVP fibers rely on thermally induced phase separation during solvent evaporation to generate interconnected pores. This distinction in pore formation mechanisms highlights the simplicity and scalability of Hb/PVP fiber fabrication, despite some trade-offs in achieving the fine pore structures characteristic of MOF-incorporated fibers.

3.2 Permeation Resistance and CO Adsorption Selectivity

The performance of multifunctional fiber membranes, such as the Hb/PVP electrospun fibers developed in this study,

relies on a delicate balance between permeation resistance and CO adsorption selectivity. These two factors often involve a trade-off, where enhancing one property may negatively impact the other, ultimately influencing the fibers' overall efficacy. Permeation resistance is primarily governed by the density, compactness, and asymmetry of the fiber matrix. The structural properties of the Hb/PVP electrospun fibers varied depending on the PVP concentration, which directly influenced the electrospinning process. For example, Hb/PVP-8 fibers, with a diameter of approximately $0.90 \pm 0.27 \mu\text{m}$ and interconnected porous structures, enabled efficient gas permeation. This was achieved by providing less tortuous diffusion pathways while maintaining mechanical stability and structural uniformity. In contrast, fibers with higher PVP concentrations, such as Hb/PVP-32 fibers, exhibited denser packing and reduced porosity. Although these characteristics enhanced structural integrity and adsorption selectivity by creating confined diffusion environments, they significantly increased permeation resistance, thereby limiting the accessibility of gas molecules to the internal fiber network [50, 51].

CO adsorption selectivity is determined by the active sites provided by Hb molecules within the fibrous matrix. The heme group in Hb strongly binds CO through specific interactions between the iron center and CO's lone electron pair. This property is critical for applications such as CO removal from the bloodstream or environmental gas capture [52]. The incorporation of PVP played a pivotal role in enhancing adsorption selectivity by improving the electrospinning process, resulting in fibers with uniform diameters and fewer defects. PVP also contributed to the formation of a stable fibrous matrix that supported Hb molecules, preventing aggregation and preserving their functional accessibility. Hb/PVP-8 fibers achieved an optimal balance by combining a high surface area-to-volume ratio with a porous structure, facilitating both gas transport and effective CO adsorption. Nevertheless, excessively high PVP concentrations, as observed in Hb/PVP-32 fibers, increased adsorption selectivity at the expense of permeability, as the densified structure restricted gas flow.

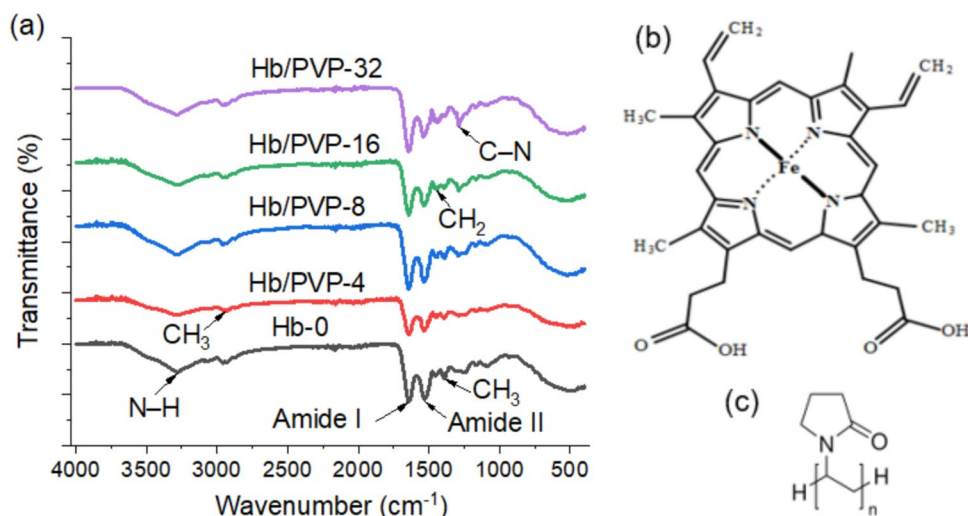
MOF-based fibers, while highly selective due to their tailored pore chemistries, often exhibit elevated permeation resistance as a result of dense packing and reduced pore interconnectivity. This limits gas diffusion and can hinder performance in dynamic adsorption systems. In contrast, Hb/PVP fibers balance permeability and adsorption. Their interconnected porous structures, combined with flexible fiber morphologies, facilitate rapid gas diffusion with minimal resistance. However, this comes at the expense of the precise CO-selective interactions that MOF-based systems excel in, making Hb/PVP fibers better suited for applications requiring fast adsorption kinetics.

The trade-off between permeation resistance and CO adsorption selectivity was evident when comparing different fiber variants. Hb-0 fibers, which lacked PVP, exhibited minimal permeation resistance due to their irregular and loosely packed morphology but demonstrated poor CO adsorption selectivity, attributed to limited active sites and structural inconsistency. Conversely, Hb/PVP-32 fibers exhibited higher selectivity due to their densified structure but suffered from increased permeation resistance, reducing their efficiency in applications that require rapid gas transfer. Hb/PVP-8 fibers emerged as an optimal compromise, achieving sufficient porosity and uniformity to enable rapid gas diffusion while maintaining a high density of exposed adsorption sites for CO. The non-linear relationship between PVP concentration and fiber performance highlights the importance of optimizing fiber properties to balance permeability and selectivity. This optimization is critical for biomedical and environmental applications, where both rapid adsorption kinetics and high selectivity are desirable. Conversely, for applications requiring prolonged exposure to CO-rich environments, such as industrial gas capture, denser fibers like Hb/PVP-32 may be more advantageous. Their excellent adsorption capacity compensates for reduced gas permeability, making them suitable for such scenarios. This relationship between permeation resistance and CO adsorption selectivity highlights the importance of tailoring the structural and compositional properties of the fibers to meet the specific demands of their intended applications.

3.3 FTIR Analysis

FTIR analysis was conducted to investigate the impact of the process on the chemical composition and to determine the characteristic functional groups present in the Hb/PVP fibers featuring different amounts of PVP. Herein, IR spectra were employed to analyze potential structural shifts in the Hb-0 electrospun fiber, along with exploring the interactions in the Hb/PVP fibers. Fig. 9 illustrates the IR spectra of Hb-0, Hb/PVP-4, -8, -16, and -32 fibers. The Hb-0 fiber exhibits identical IR spectral characteristics to those of Hb/PVP fibers, indicating that the Hb/PVP fibers possessed nearly identical functional group. The IR spectra of all Hb fibers show distinct peaks that reflect Amide I and II bands, which are 1665 and 1550 cm^{-1} , respectively. In general, the IR spectrum of Hb, the structure of which is revealed in Fig. 9b, primarily shows the absorption of peptide bonds. The 1680 – 1620 cm^{-1} range corresponds to the C=O stretching vibration of the peptide backbone, comprising the Amide I band. C–N stretching and N–H bending vibrations contribute to the 1560 – 1520 cm^{-1} range, forming the Amide II band [53]. Furthermore, the absorption band occurs around

Fig. 9 a IR spectra of Hb-0, Hb/PVP-4, -8, -16, -32 fibers, (b) hemoglobin structure [61], and (c) PVP structure [62]



3300 cm^{-1} in the IR spectrum and is associated with the stretching vibration of the N–H bond of Amide A (primary amide).

The IR spectra of Amide suggest the presence of numerous fine components within the amide structure. Each chemical group contributes independently to the amide I, II, and A bands, with varying degrees of influence [54]. Peaks observed at $2961\text{--}2874\text{ cm}^{-1}$ and 1396 cm^{-1} correspond to the $-\text{CH}_3$ asymmetric stretching and $-\text{CH}_3$ symmetric bending vibrations, respectively [55]. The peak observed within the range of $3000\text{--}4000\text{ cm}^{-1}$ in IR spectra is associated with the hydroxyl $-\text{OH}$ elastic vibration as the wt. % of PVP increases in Hb fibers, characteristic bands of PVP, the structure of which is shown in Fig. 9c, starts to display [56]. PVP is a branched polymer, which has a structure that is more complex than linear polymers yet remains confined to a two-dimensional plane [57]. In addition to sharing common functional groups with Hb electrospun fibers such as C=O stretching and N–H bending vibrations, PVP also demonstrates vibrations associated with $-\text{CH}_2$ bending and $-\text{C}-\text{N}$ stretching, showing at the $1450\text{--}1470\text{ cm}^{-1}$ range and 1290 cm^{-1} , respectively [58, 59].

Furthermore, the IR spectra exhibit peaks at 1447 cm^{-1} , which are assigned to the hydroxyl $-\text{OH}$ bending vibrations. The peaks observed at 2900 cm^{-1} correspond to the C–H stretching vibration. Notably, the peak observed at 1630 cm^{-1} for Hb-0 fiber is associated with the C=O stretching vibration, which has shifted to 1518 cm^{-1} in the case of Hb/PVP electrospun fibers, implying the presence of interaction between the C=O groups of Hb and PVP within the Hb/PVP fiber [60]. In summary, the FTIR analysis revealed the existence of molecular interactions between the Hb and PVP matrix within the electrospun fiber.

3.4 TGA and DSC Analysis

Thermal analysis techniques such as TGA play a vital role in the characterization of Hb/PVP fibers. The TGA provides a valuable source of information regarding crucial parameters related to the performance of electrospun fibers, including their thermal stability, the ratio of the volatile component, the onset temperature of decomposition, and the magnitude of weight loss as the electrospun fibers engage in the heating process at a constant heating rate [63]. Adequate thermal stability is essential for ensuring that electrospun fibers can endure at different temperatures. Heat transfer mechanisms and medium diffusion processes may be used to elucidate this phenomenon. Derivative Thermogravimetric (DTG) analysis is utilized to specify the precise temperature at which the electrospun fibers experience their most significant weight loss [64].

Meanwhile, TGA assesses thermal stability and indicates degradation temperatures. DSC identifies phase transitions like denaturation and melting, aiding in understanding structural changes and physical states. These analyses inform decisions regarding thermal processing and exposure to elevated temperatures. Figs. 10 and 11 show the thermal behavior of all Hb-based samples produced in this study. It appears that adding PVP to Hb electrospun fibers did have a slight effect on the overall reaction of electrospun fibers under heat. Fig. 10 presents the TGA and DTG profiles of fibers prepared from a combination of Hb and different concentrations of PVP, delineating three distinct stages of weight loss. Blue lines depict the TGA curve, which displays the weight loss of each electrospun fiber as a function of temperature. Red lines depict the DTG curve, which illustrates the rate of weight loss for each electrospun fiber over time.

At the first stage of TGA, there is a DTG peak at around $32\text{ }^\circ\text{C}$ for all Hb-0 and Hb/PVP samples, suggesting a similar

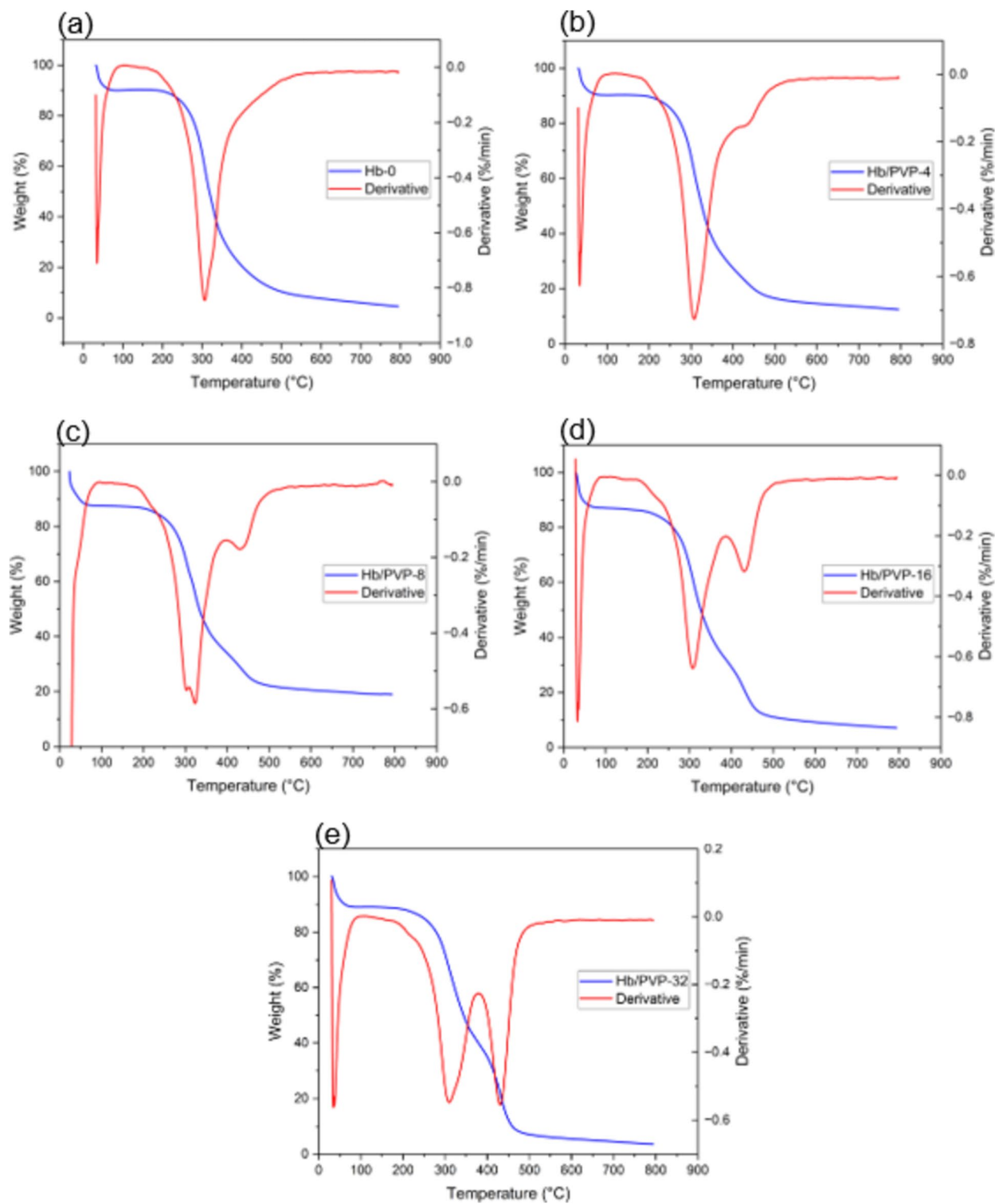


Fig. 10 TGA and DTG plots of (a) Hb-0, (b) Hb/PVP-4, (c) Hb/PVP-8, (d) Hb/PVP-16, and (e) Hb/PVP-32 fibers

phenomenon occurring in all samples. This peak likely corresponds to the removal of moisture or other volatile components that are physically or chemically bound within the fiber structure. At temperatures around 32 °C, these volatile

components begin to evaporate or desorb from the surface or interior of the nanofibers, leading to a noticeable weight loss. The TGA graphs show that for all Hb-0 and Hb/PVP samples, the temperature range at which 10% weight loss is

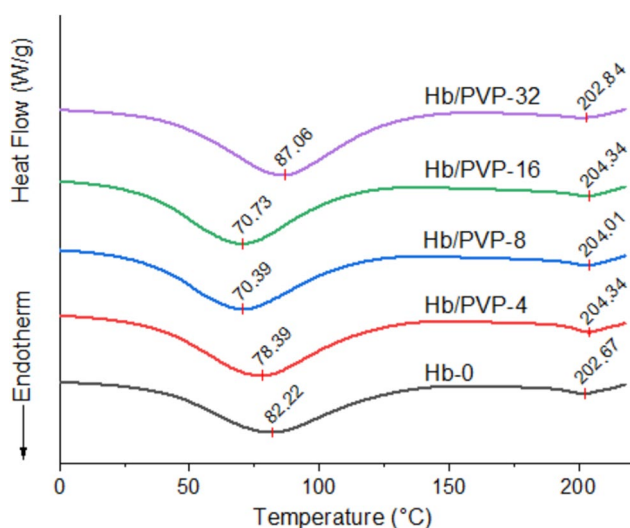


Fig. 11 DSC plots of Hb-0, Hb/PVP-4, -8, -16, and -32 fibers

observed is approximately the same, indicating that the addition of PVP does not significantly alter the moisture content or the nature of volatile components within the nanofiber samples. This suggests that the interaction between Hb and PVP at this stage may not strongly influence the behavior of moisture desorption or volatile component release.

DSC curves of all fibers also have endothermic peak around 80 °C. To be more specific, Hb-0, Hb/PVP-4, -8, 16, and -32 fibers have endothermic peaks of 82.22 °C, 78.39 °C, 70.39 °C, 70.73 °C, and 87.06 °C, respectively, as shown in Fig. 2. These peaks indicate denaturation or aggregation of Hb. It is a common phenomenon in thermal energy that causes the native structure of Hb to destabilize. Heat can disrupt the weak intermolecular forces holding the protein structure together, leading to unfolding or loss of conformation. This process, referred to as Hb denaturation [65], has been observed to occur ultimately around 80 °C [66]. Hb is a protein composed of four subunits, and while exposed to heat, the denaturation of Hb is characterized by cooperation among these subunits. In other words, one subunit influences and is influenced by other subunits, resulting in a synchronized transition of the entire protein structure because of heat [67].

The straight line observed in the TGA curve of all samples from 70 to 200 °C suggests a stage of thermal stabilization or minimal weight loss within this temperature range. This period corresponds to a stabilization stage, during which moderate heat is applied to the fibers to remove residual solvents, moisture, or volatile components, thereby enhancing their structural integrity and stability. The absence of significant weight loss during this phase indicates that the fibers are relatively stable and not undergoing substantial decomposition or degradation. Additionally, the straight line may signify consistent heating conditions, or a

steady heating rate maintained throughout the TGA experiment, ensuring controlled and accurate characterization of the thermal behavior of the fibers.

In the second stage of TGA, which spans from 200 to 450 °C, a notable weight loss of approximately 80% was observed, indicating the degradation of amino acids and PVP, which aligns with gradual incline of TGA curve around 200–300 °C, indicating the degradation of amino acids [68]. This inference finds support in the presence of an endothermic peak detected around 202–204 °C on the DSC graph, as well as a corresponding DTG peak at approximately 300 °C across all samples. Additionally, a notable shift is observed at this stage, as indicated by the presence of only one DTG peak around 300 °C on the TGA graph of Hb-0 fiber, implying thermal degradation of hemoglobin. However, with the introduction of PVP into Hb fibers, a second DTG peak emerges around 430 °C, indicating thermal degradation of PVP. Notably, as the concentration of PVP increases, this second peak becomes more pronounced, as depicted in Figs. 10b, c, d and e.

It was suggested that PVP starts to degrade above 300 °C, with significant weight loss occurring around 430 °C due to the degradation of the PVP main chain [69, 70]. All the samples in the last stage, which is beyond 430 °C, remained as residue ash, yielding the completion of material degradation. The increment of PVP into the Hb-based electrospun multifunctional micro- and nanofibers demonstrated a reduction in thermal stability for Hb/PVP fibers. The noticeable weight loss observed from the electrospun fibers by heating can be attributed to the removal of volatiles deriving from complex chemical reactions such as cyclization, dehydrogenation, and cross-linking processes [25].

3.5 Water Contact Angle Analysis

The water contact angle (WCA) analysis was employed to investigate the wettability of Hb)-based electrospun multifunctional micro- and nanofibers, which is a critical component of the CO absorption process. WCA is a key parameter used to assess the hydrophobicity or hydrophilicity of the resulting fibers. Understanding the WCA of Hb/PVP fibers is essential for tailoring their surface characteristics to specific applications. In this study, WCA values of Hb-0 fibers and Hb fibers with different concentrations of PVP were measured at 40, 200, and 400-second time frames. The hydrophobic behavior of pristine Hb-0 fibers observed in the WCA analysis, where WCA value remains close to 120° after 400 seconds, may initially seem contradictory given that Hb is inherently hydrophilic due to its functional groups, as shown in Fig. 9b, such as hydroxyl (-OH), amino (-NH₂), and carboxyl (-COOH), are partially negative due to the higher electronegativity of oxygen and nitrogen atoms compared to carbon and hydrogen atoms. This property

facilitates the formation of hydrogen bonds with the partially positive hydrogen atoms of water molecules.

Electrospinning alters the physical arrangement and surface exposure of Hb molecules. In Hb-0 fibers, Hb molecules are tightly packed and stabilized in a globular conformation, limiting the accessibility of their hydrophilic functional groups on the fiber surface. This dense molecular arrangement reduces the availability of hydrogen bonding sites for interaction with water molecules. Additionally, during the electrospinning process, solvent retention within the fibers and rapid solvent evaporation can induce surface densification, forming a relatively smooth, compact surface layer. This compact surface minimizes the fiber's ability to interact with water, further contributing to the observed hydrophobic behavior. The ribbon-like morphology of Hb-0 fibers, as revealed in CLSM imaging, also plays a significant role. These deformed, flattened fibers result from solvent evaporation and polymer relaxation during the electrospinning process, which creates a surface that may resist water spreading. The lack of porosity in these fibers further limits water penetration into the fiber interior, thereby reinforcing the hydrophobicity. In contrast to porous and rough surfaces, smooth, dense surfaces naturally exhibit higher WCA values due to reduced capillary forces that would otherwise draw water into the structure.

Another factor contributing to this behavior is the intrinsic limitation of pure Hb as a polymeric system for electrospinning. Hb lacks long-chain entanglement and the molecular flexibility required to form robust fibrous networks. This deficiency often leads to inconsistencies in fiber morphology and mechanical stability, resulting in less effective interaction with water, and without the support of a carrier polymer, such as PVP, the Hb-0 fibers fail to achieve the hydrophilic surface properties typically associated with Hb in solution. PVP not only stabilizes the electrospinning process but also enhances the exposure of hydrophilic functional groups by increasing the flexibility and spinnability of the polymer solution [71]. The absence of PVP in Hb-0 fibers thus limits their hydrophilicity, further contributing to the high WCA values observed. The synergistic effect between the hydrophilic functional groups of Hb and PVP significantly increased the fibers' ability to absorb water, as reflected by the progressively lower WCA values observed in fibers with increasing PVP concentrations [72, 73].

Furthermore, Hb/PVP-16 and Hb/PVP-32 fibers demonstrated a significant transition from hydrophobic to hydrophilic behavior at early time points, as illustrated in Fig. 12. At 40 seconds, Hb/PVP-16 fiber exhibited a WCA of $72.49 \pm 0.24^\circ$, while Hb/PVP-32 fiber showed a slightly higher WCA of $76.47 \pm 3.16^\circ$. The surface effects of higher PVP concentrations can explain this higher initial WCA for Hb/PVP-32 fiber. As PVP content increases, the surface becomes saturated with hydrophilic groups, leading to

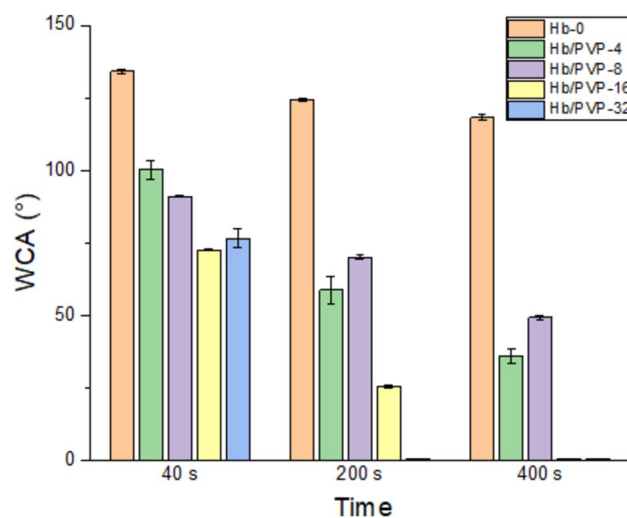


Fig. 12 The hydrophilic transition of Hb-0, Hb/PVP-4, -8, 16, and -32 fibers from 40 to 400 seconds

localized polymeric packing that transiently hinders water spreading by creating a denser barrier at the fiber-air interface. Additionally, excessive PVP can alter the microstructure of the fiber surface, potentially introducing regions of lower porosity and reducing immediate accessibility to hydrophilic functional groups. However, these effects are transient, as the highly porous network of Hb/PVP-32 fiber facilitates rapid water penetration beyond this initial phase. By 200 seconds, Hb/PVP-32 fiber achieved complete water absorption, with a WCA of less than 5° , indicating a complete transition to superhydrophilicity. In comparison, Hb/PVP-16 fiber exhibited a similar hydrophilic state only after 400 seconds, suggesting that the higher PVP concentration in Hb/PVP-32 fiber provided an enhanced capacity for hydrogen bonding and faster water uptake.

Lower PVP concentration fibers, such as Hb/PVP-4 and Hb/PVP-8 fibers, showed slower transitions to hydrophilicity. Hb/PVP-4 fiber exhibited WCA values of $100.18 \pm 3.25^\circ$, $58.67 \pm 4.67^\circ$, and $35.88 \pm 2.30^\circ$ at 40, 200, and 400 seconds, respectively, while Hb/PVP-8 fiber showed values of $90.98 \pm 0.14^\circ$, $69.91 \pm 0.66^\circ$, and $49.21 \pm 0.69^\circ$ over the same timeframe. These higher WCA values at all time points reflect the reduced density of hydrophilic functional groups at lower PVP concentrations, resulting in slower water spreading and absorption. Interestingly, Hb/PVP-4 fiber demonstrated faster water absorption compared to Hb/PVP-8 fiber despite having a lower PVP concentration that can be attributed to differences in fiber porosity and packing density induced by variations in PVP concentration during electrospinning. At lower PVP concentrations, such as in Hb/PVP-4 fiber, the polymer chains exhibit reduced entanglement, leading to a less stable electrospinning jet. This instability often results in a more loosely packed fiber mat

with larger void spaces and higher porosity. The increased porosity allows water molecules to infiltrate the fiber network more readily, enhancing water absorption.

In contrast, the slightly higher PVP concentration in Hb/PVP-8 fiber likely increases chain entanglement and solution viscosity, stabilizing the electrospinning process. This stabilization leads to a denser fiber mat with reduced void spaces, which can delay water penetration despite the fibers being naturally more hydrophilic. These findings highlight the complex interplay between fiber morphology, porosity, and hydrophilicity in determining water absorption behavior. Conversely, pristine Hb-0 fibers maintained their hydrophobic nature throughout the observation period, with a WCA of $118.26 \pm 1.12^\circ$ even after 400 seconds. This result emphasizes the inherent limitations of pure Hb fibers in facilitating efficient water absorption due to their lack of hydrophilic network formation.

The relationship between fiber morphology, porosity, and PVP concentration plays a crucial role in determining wettability. Higher PVP concentrations contribute to greater chain entanglement during electrospinning, resulting in a more uniform and porous fiber network. The porosity in Hb/PVP-32 fiber enhances water penetration by providing interconnected pathways for water molecules to access internal hydrophilic functional groups. However, the slight delay in water absorption observed for Hb/PVP-32 fiber at 40 seconds highlights the need to optimize polymer concentrations to balance immediate wettability with structural integrity. The rapid transition to hydrophilicity observed in Hb/PVP-32 and Hb/PVP-16 fibers is particularly advantageous for CO absorption applications, as it ensures efficient interaction with aqueous environments, allowing CO molecules to diffuse into the fiber matrix for effective adsorption. Table 2 shows the detailed WCAs between 40 and 400 seconds of Hb/PVP fibers developed for CO absorption in the bloodstream. Overall, it is concluded that the present study may open new possibilities to increase the absorption rate of highly porous, flexible and multifunctional fibers for CO absorption in the bloodstream and address the concerns.

The Hb-based electrospun multifunctional fibers developed in this study demonstrate a range of critical functions, emphasizing their versatility and suitability for CO capturing

and broader biomedical and environmental applications. The primary function of these fibers is efficient CO absorption, achieved through the high gas-binding affinity of Hb, whose heme group iron binds CO approximately 250 times more strongly than oxygen. This property positions the fibers as biomimetic materials for effective CO capture in physiological or environmental settings. Another critical function of these fibers is their hydrophilicity, attributed to the inclusion of PVP, which exhibits strong interactions with water molecules through its electronegative oxygen and nitrogen atoms. WCA measurements confirm the fibers' enhanced wettability, with those containing higher PVP concentrations (16 and 32 wt.%) achieving complete water absorption within 200 seconds. This rapid transition to hydrophilicity is essential for compatibility with aqueous environments, such as blood or other biological fluids, where CO is dissolved. The hydrophilic nature of the fibers also ensures that Hb retains its functional integrity in wet conditions, promoting the effective interaction of CO molecules with active heme sites. Thermal stability was another notable characteristic, with consistent phase transition behavior observed across different PVP concentrations. Hb denatured around 80°C , and significant degradation occurred between 200°C and 430°C , demonstrating robustness for various applications. The mechanical stability of the fibers is enhanced by PVP, which acts as a carrier polymer, enabling the fabrication of continuous, uniform fibers free of defects like beads, which is critical for ensuring functional and structural integrity. Additionally, the biocompatibility of Hb and PVP ensures that these flexible fibers are non-toxic and suitable for biomedical use, particularly in scenarios involving CO removal from blood circulation. These combined properties highlight the fibers' multifunctionality and scalability, enabling their adaptation for diverse applications through adjustments in PVP concentration (or other polymers) and electrospinning parameters.

4 Conclusions

This study successfully developed Hb-based electrospun multifunctional fibers with PVP, aimed at creating advanced materials for CO capture. By varying PVP concentrations, continuous, uniform, and flexible fibers with varying diameters were produced, demonstrating the versatility of electrospinning as a fabrication technique. Morphological analysis using confocal laser scanning microscopy revealed the micron- and nanoscale structures of the electrospun fibers. Additionally, FTIR spectroscopy identified the composition and chemical characteristics of the composite nanofibers, while TGA and DSC analyses provided insights into their thermal properties and phase transitions. Among the samples tested, Hb-based electrospun fibers containing 8 wt.% PVP exhibited desirable morphology with micron- and submicron-scale diameters. The samples

Table 2 Water contact angles of Hb/PVP fibers developed for CO absorption in the bloodstream

Sample	Water Contact Angle ($^\circ$)		
	40-second	200-second	400-second
Hb-0	134.06 ± 0.86	124.31 ± 0.65	118.26 ± 1.12
Hb/PVP-4	100.18 ± 3.25	58.67 ± 4.67	35.88 ± 2.30
Hb/PVP-8	90.98 ± 0.14	69.91 ± 0.66	49.21 ± 0.69
Hb/PVP-16	72.49 ± 0.24	25.51 ± 0.59	<5
Hb/PVP-32	76.47 ± 3.16	<5	<5

with 16 and 32 wt.% PVP displayed the highest hydrophilicity, fully absorbing water after 400 and 200 seconds, respectively. All fibers exhibited critical thermal transitions at approximately 80 °C, corresponding to Hb denaturation, and around 200 °C, where decomposition into constituent amino acids began, with significant degradation observed between 200 and 430 °C. This study primarily focused on the development and characterization of Hb-based electrospun PVP fibers. While foundational properties of these materials were successfully established, their specific CO-capturing capacity and kinetics remain unexplored and warrant further investigation. Future research should aim to quantify the CO uptake performance of these fibers under controlled environmental conditions, including variations in temperature, pressure, and humidity, to validate their practical applicability. Additionally, studies on the molecular interactions between Hb and CO within the fibrous matrix would provide valuable insights for enhancing material performance. The potential hybridization of MOFs with Hb/PVP fibers presents an exciting avenue for future research, offering a strategy to combine the strengths of both systems. Such hybrid fibers could address current limitations, expanding the applicability of multifunctional membranes in CO adsorption and beyond. Finally, long-term stability studies examining the durability of these fibers under operational conditions are essential to establish their viability as advanced materials for CO capture. Addressing these research gaps will bridge the existing knowledge divide and pave the way for transformative advancements in biomedical and environmental material sciences.

Author Contribution A.P.: Investigation, data curation, methodology, writing—original draft, review, and editing; B.S.: Methodology, writing—review and editing; E.A.: Methodology, writing—review and editing; R.A.: Conceptualization, data curation, methodology, writing—review and editing, supervision.

Funding Not applicable.

Data Availability No datasets were generated or analysed during the current study.

Declarations

Ethical Approval Not applicable.

Conflict of Interest The authors declare no competing interests.

Open Access This article is licensed under a Creative Commons Attribution 4.0 International License, which permits use, sharing, adaptation, distribution and reproduction in any medium or format, as long as you give appropriate credit to the original author(s) and the source, provide a link to the Creative Commons licence, and indicate if changes were made. The images or other third party material in this article are included in the article's Creative Commons licence, unless indicated otherwise in a credit line to the material. If material is not included in the article's Creative Commons licence and your intended use is not permitted by statutory regulation or exceeds the permitted use, you will

need to obtain permission directly from the copyright holder. To view a copy of this licence, visit <http://creativecommons.org/licenses/by/4.0/>.

References

- Rose, J. J., Wang, L., Xu, Q., McTiernan, C. F., Shiva, S., Tejero, J., & Gladwin, M. T. (2017). Carbon monoxide poisoning: Pathogenesis, management, and future directions of therapy. *American Journal of Respiratory and Critical Care Medicine*, *195*, 596–606. <https://doi.org/10.1164/rccm.201606-1275CI>
- Nazarian, D. J., Eddy, O. L., Lukens, T. W., Weingart, S. D., & Decker, W. W. (2009). Clinical Policy: Critical Issues in the Management of Adult Patients Presenting to the Emergency Department With Community-Acquired Pneumonia. *Annals of Emergency Medicine*, *54*, 704–731. <https://doi.org/10.1016/j.annemergmed.2009.07.002>
- Zevin, S., Saunders, S., Gourlay, S. G., Jacob, P., & Benowitz, N. L. (2001). Cardiovascular effects of carbon monoxide and cigarette smoking. *Journal of the American College of Cardiology*, *38*, 1633–1638. [https://doi.org/10.1016/S0735-1097\(01\)01616-3](https://doi.org/10.1016/S0735-1097(01)01616-3)
- Pitto-Barry, A., Lupan, A., Ellingford, C., Attia, A. A. A., & Barry, N. P. E. (2018). New Class of Hybrid Materials for Detection, Capture, and “on-Demand” Release of Carbon Monoxide. *ACS Applied Materials & Interfaces*, *10*, 13693–13701. <https://doi.org/10.1021/acsami.8b01776>
- Ma, X., Albertsma, J., Gabriels, D., Horst, R., Polat, S., Snoeks, C., Kapteijn, F., Eral, H. B., Vermaas, D. A., & Mei, B. (2023). others, Carbon monoxide separation: Past, present and future. *Chemical Society Reviews*, *52*, 3741–3777.
- Uddin, M. N., Rahman, M. M., & Asmatulu, E. (2020). Sustainable freshwater harvesting from atmosphere through nanocomposite fibers of recycled polystyrene foams. In *Behavior and Mechanics of Multifunctional Materials IX* (Vol. 11377, pp. 183–191). SPIE. <https://doi.org/10.1117/12.2563401>.
- Uddin, M. N., Desai, F. J., Subeshan, B., Rahman, M. M., & Asmatulu, E. (2021). Sustainable atmospheric fog water generator through superhydrophobic electrospun nanocomposite fibers of recycled expanded polystyrene foams. *Surfaces and Interfaces*, *25*, 101169. <https://doi.org/10.1016/j.surfin.2021.101169>
- Koyun, M., Sulutas, R. B., Turan, Y., Karabulut, H., Moradi, A., Ozarici, H. B., Ulag, S., Sahin, A., Guncu, M. M., & Gunduz, O. (2023). Electrospun composite nanofibers for treating infectious esophagitis. *Emergent Materials*, *6*, 1549–1561. <https://doi.org/10.1007/s42247-023-00533-9>
- Uddin, M. N., Desai, F. J., Rahman, M. M., & Asmatulu, R. (2020). A highly efficient fog harvester of electrospun permanent superhydrophobic-hydrophilic polymer nanocomposite fiber mats. *Nanoscale Advances*, *2*, 4627–4638. <https://doi.org/10.1039/d0na00529k>
- Subeshan, B., Atayo, A., & Asmatulu, E. (2024). Machine learning applications for electrospun nanofibers: A review. *Journal of Materials Science*, *59*, 14095–14140. <https://doi.org/10.1007/s10853-024-09994-7>
- Hussain, M. H., Abu Bakar, N. F., Chung, M., Khalid, N. F. N., Othman, N. H., Tan, H. L., Osman, M. S., Lockman, Z., & Radacsi, N. (2023). Electrospun polyetherimide nanofibers with reduced graphene oxide-zeolitic imidazolate framework for conductivity improvement. *Emergent Materials*, *6*, 271–281. <https://doi.org/10.1007/s42247-022-00410-x>
- Shang, H., Xu, K., Li, T., Yang, H. R., Gao, J., Li, S., Zhu, J., He, X., Zhang, S., Xu, H., & Shen, B. (2023). Bioelectret poly(lactic acid) membranes with simultaneously enhanced physical interception and electrostatic adsorption of airborne PM0.3. *Journal*

- of *Hazardous Materials*, 458, 132010. <https://doi.org/10.1016/j.jhazmat.2023.132010>
13. Zhu, G., Wang, C., Yang, T., Gao, N., Zhang, Y., Zhu, J., He, X., Shao, J., Li, S., Zhang, M., Zhang, S., Gao, J., & Xu, H. (2024). Bio-inspired gradient poly(lactic acid) nanofibers for active capturing of PM0.3 and real-time respiratory monitoring. *Journal of Hazardous Materials*, 474, 134781. <https://doi.org/10.1016/j.jhazmat.2024.134781>
 14. Jiang, L., Zhu, X., Li, J., Shao, J., Zhang, Y., Zhu, J., Li, S., Zheng, L., Li, X. P., Zhang, S., Li, H., Zhong, G. J., & Xu, H. (2024). Electroactive and breathable protective membranes by surface engineering of dielectric nanohybrids at poly(lactic acid) nanofibers with excellent self-sterilization and photothermal properties. *Separation and Purification Technology*, 339, 126708. <https://doi.org/10.1016/j.seppur.2024.126708>
 15. Song, X., He, X., Tang, M., Wang, C., Zhang, Y., Li, X., Li, T., Ke, L., Li, X., Zhang, M., Zhang, S., & Xu, H. (2024). Multi-Protection from Microbial and PM Pollutants by Humidity-Resistant, Breathable and Self-Charging Nanofibrous Membranes. *ACS Sustainable Chemistry & Engineering*, 12, 12216–12225. <https://doi.org/10.1021/acsschemeng.4c04333>
 16. Li, Y., Zhu, J., Cheng, H., Li, G., Cho, H., Jiang, M., Gao, Q., & Zhang, X. (2021). Developments of Advanced Electrospinning Techniques: A Critical Review. *Advanced Materials Technologies*, 6, 2100410. <https://doi.org/10.1002/admt.202100410>
 17. Uddin, M. N., Desai, F. J., & Asmatulu, E. (2020). Biomimetic electrospun nanocomposite fibers from recycled polystyrene foams exhibiting superhydrophobicity. *Energy, Ecology and Environment*, 5, 1–11. <https://doi.org/10.1007/s40974-019-00140-7>
 18. Naragund, V. S., & Panda, P. K. (2022). Electrospun nanofiber-based respiratory face masks—a review. *Emergent Materials*, 5, 261–278. <https://doi.org/10.1007/s42247-022-00350-6>
 19. Ijaola, A. O., Mohammed, Q. S., Obi, M., Akamo, D. O., Ajiboye, E. G., Twomey, J., Yang, S. Y., & Asmatulu, E. (2024). Hydrophilic and Antibacterial Electrospun Nanofibers from Monofilament Fishing Lines. *Fibers Polymers*, 25, 59–69. <https://doi.org/10.1007/s12221-023-00428-w>
 20. Baddam, Y., Ijaola, A. O., & Asmatulu, E. (2021). Fabrication of flame-retardant and superhydrophobic electrospun nanofibers. *Surfaces and Interfaces*, 23, 101017. <https://doi.org/10.1016/j.surfin.2021.101017>
 21. Ahmed, T., Mohammed, Q., Subeshan, B., Rahman, M., Nuraje, N., & Asmatulu, E. (2022). Improving flame retardancy and hydrophobicity of fabrics via graphene inclusion obtained from recycled batteries. *Materials Today: Proceedings*, 71, 78–89. <https://doi.org/10.1016/j.matpr.2022.07.469>
 22. Rahmati, M., Mills, D. K., Urbanska, A. M., Saeb, M. R., Venugopal, J. R., Ramakrishna, S., & Mozafari, M. (2021). Electrospinning for tissue engineering applications. *Progress in Materials Science*, 117, 100721. <https://doi.org/10.1016/j.pmatsci.2020.100721>
 23. Calderón, J. C., García, G., Querejeta, A., Alcaide, F., Calvillo, L., Lázaro, M. J., Rodríguez, J. L., & Pastor, E. (2015). Carbon monoxide and methanol oxidations on carbon nanofibers supported Pt-Ru electrodes at different temperatures. *Electrochimica Acta*, 186, 359–368. <https://doi.org/10.1016/j.electacta.2015.09.121>
 24. Yang, J., Zhou, H., Wang, L., Zhang, Y., Chen, C., Hu, H., Li, G., Zhang, Y., Ma, Y., & Zhang, J. (2017). Cobalt-Doped K-OMS-2 Nanofibers: A Novel and Efficient Water-Tolerant Catalyst for the Oxidation of Carbon Monoxide. *ChemCatChem*, 9, 1163–1167. <https://doi.org/10.1002/cctc.201601681>
 25. Eid, K., Sliem, M. H., Eldesoky, A. S., Al-Kandari, H., & Abdullah, A. M. (2019). Rational synthesis of one-dimensional carbon nitride-based nanofibers atomically doped with Au/Pd for efficient carbon monoxide oxidation. *International Journal of Hydrogen Energy*, 44, 17943–17953. <https://doi.org/10.1016/j.ijhydene.2019.05.105>
 26. X. Liu, S. Jia, M. Yang, Y. Tang, Y. Wen, S. Chu, J. Wang, B. Shan, R. Chen, Author Correction: Activation of subnanometric Pt on Cu-modified CeO₂ via redox-coupled atomic layer deposition for CO oxidation (Nature Communications, (2020), 11, 1, (4240), <https://doi.org/10.1038/s41467-020-18076-6>), Nat. Commun. 11 (2020) 4240. <https://doi.org/10.1038/s41467-020-19663-3>.
 27. Sargazi, G., Afzali, D., Mostafavi, A., Shadman, A., Rezaee, B., Zarrintaj, P., Saeb, M. R., Ramakrishna, S., & Mozafari, M. (2019). Chitosan/polyvinyl alcohol nanofibrous membranes: Towards green super-adsorbents for toxic gases. *Heliyon*, 5, e01527. <https://doi.org/10.1016/j.heliyon.2019.e01527>
 28. Ravichandran, R., Seitz, V., Reddy Venugopal, J., Sridhar, R., Sundarajan, S., Mukherjee, S., Wintermantel, E., & Ramakrishna, S. (2013). Mimicking Native Extracellular Matrix with Phytic Acid-Crosslinked Protein Nanofibers for Cardiac Tissue Engineering. *Macromolecular Bioscience*, 13(366), 366–375. <https://doi.org/10.1002/mabi.201200391>
 29. Sahtani, K., Aykut, Y., & AladagTanik, N. (2022). Hemoglobin assisted carbon nanofiber preparation for selective detection of miRNA molecules. *Journal of Industrial Textiles*, 51, 4514S–4539S. <https://doi.org/10.1177/15280837211049566>
 30. Wu, J. P., & Yin, F. (2013). Novel Hydrogen Peroxide Biosensor Based on Hemoglobin Combined with Electrospinning Composite Nanofibers. *Analytical Letters*, 46, 818–830. <https://doi.org/10.1080/00032719.2012.733900>
 31. Tabassum, M., Zia, Q., Li, J., Khawar, M. T., Aslam, S., & Su, L. (2023). FAPbBr 3 Perovskite Nanocrystals Embedded in Poly(L-lactic acid) Nanofibrous Membranes for Enhanced Air and Water Stability. *Membranes (Basel)*, 13, 279. <https://doi.org/10.3390/membranes13030279>
 32. Lerond, M., Subramanian, A., Skene, W. G., & Cicaira, F. (2021). Combining Electrospinning and Electrode Printing for the Fabrication of Stretchable Organic Electrochemical Transistors. *Frontiers in Physics*, 9, 708914. <https://doi.org/10.3389/fphy.2021.708914>
 33. Ma, G. P., Yang, D. Z., Ling Chen, B., Ding, S. M., Song, G. Q., & Nie, J. (2010). Preparation and characterization of composite fibers from organic-soluble chitosan and poly-vinylpyrrolidone by electrospinning. *Frontiers of Materials Science in China*, 4, 64–69. <https://doi.org/10.1007/s11706-010-0012-5>
 34. Jie, B., Yaoxian, L., Lei, S., Chaoqun, Z., & Qingbiao, Y. (2009). Bicomponent AgCl/PVP nanofiber fabricated by electrospinning with gel-sol method. *Bulletin of Materials Science*, 32, 161–164. <https://doi.org/10.1007/s12034-009-0024-x>
 35. Blumenthal, I. (2001). Carbon monoxide poisoning. *Journal of the Royal Society of Medicine*, 94, 270–272. <https://doi.org/10.1177/014107680109400604>
 36. Perutz, M. F. (1990). Mechanisms regulating the reactions of human hemoglobin with oxygen and carbon monoxide. *Annual Review of Physiology*, 52, 1–25. <https://doi.org/10.1146/annurev.physiol.52.1.1>
 37. Raven, P. H., Johnson, G. B., & Mason, K. A. (2011). *Biology*. McGraw-Hill.
 38. Peng, J.-B., Geng, H.-Q., & Wu, X.-F. (2019). The chemistry of CO: Carbonylation. *Chem*, 5, 526–552.
 39. Lemon, B. J., & Peters, J. W. (1999). Binding of exogenously added carbon monoxide at the active site of the iron-only hydrogenase (CpI) from *Clostridium pasteurianum*. *Biochemistry*, 38, 12969–12973. <https://doi.org/10.1021/bi9913193>
 40. Olson, J. S., Mathews, A. J., Rohlfs, R. J., Springer, B. A., Egeberg, K. D., Sligar, S. G., Tame, J., Renaud, J. P., & Nagai, K. (1988). The role of the distal histidine in myoglobin and haemoglobin. *Nature*, 336, 265–266. <https://doi.org/10.1038/336265a0>

41. Levy, A., Sharma, V. S., Zhang, L., & Rifkind, J. M. (1992). A new mode for heme-heme interactions in hemoglobin associated with distal perturbations. *Biophysical Journal*, *61*, 750–755. [https://doi.org/10.1016/S0006-3495\(92\)81879-9](https://doi.org/10.1016/S0006-3495(92)81879-9)
42. Barnes, C. P., Smith, M. J., Bowlin, G. L., Sell, S. A., Tang, T., Matthews, J. A., Simpson, D. G., & Nimitz, J. C. (2006). Feasibility of Electrospinning the Globular Proteins Hemoglobin and Myoglobin. *Journal of Engineered Fibers and Fabrics*, *1*, 155892500600100. <https://doi.org/10.1177/155892500600100202>
43. Koombhongse, S., Liu, W., & Reneker, D. H. (2001). Flat polymer ribbons and other shapes by electrospinning. *Journal of Polymer Science Part B: Polymer Physics*, *39*, 2598–2606. <https://doi.org/10.1002/polb.10015>
44. Woerdeman, D. L., Shenoy, S., & Breger, D. (2007). Role of chain entanglements in the electrospinning of wheat protein-poly(vinyl alcohol) blends. *The Journal of Adhesion*, *83*, 785–798. <https://doi.org/10.1080/00218460701588398>
45. Nie, H., He, A., Zheng, J., Xu, S., Li, J., & Han, C. C. (2008). Effects of chain conformation and entanglement on the electrospinning of pure alginate. *Biomacromolecules*, *9*, 1362–1365. <https://doi.org/10.1021/bm701349j>
46. Hu, X., He, J., Zhu, L., Machmudah, S., Wahyudiono, H., & Kanda, M. Goto. (2022). Synthesis of Hollow PVP/Ag Nanoparticle Composite Fibers via Electrospinning Under A Dense CO₂ Environment. *Polymers (Basel)*, *14*, 89. <https://doi.org/10.3390/polym14010089>
47. Cao, X., Chen, W., Zhao, P., Yang, Y., & Yu, D. G. (2022). Electrospun Porous Nanofibers: Pore-Forming Mechanisms and Applications for Photocatalytic Degradation of Organic Pollutants in Wastewater. *Polymers (Basel)*, *14*, 3990. <https://doi.org/10.3390/polym14193990>
48. Grant, J. J., Pillai, S. C., Perova, T. S., Hehir, S., Hinder, S. J., McAfee, M., & Breen, A. (2021). Electrospun fibres of chitosan/PVP for the effective chemotherapeutic drug delivery of 5-fluorouracil. *Chemosensors*, *9*, 70. <https://doi.org/10.3390/chemosensors9040070>
49. K. Nasouri, A.M. Shoushtari, M.R.M. Mojtahedi (2015) Thermodynamic Studies on Polyvinylpyrrolidone Solution Systems Used for Fabrication of Electrospun Nanostructures: Effects of the Solvent. *Advances in Polymer Technology* *34*. <https://doi.org/10.1002/adv.21495>.
50. Hazarika, G., & Ingole, P. G. (2024). Nano-enabled gas separation membranes: Advancing sustainability in the energy-environment Nexus. *Science of The Total Environment*, *944*, 173264.
51. Liu, S., Jassby, D., Mandler, D., & Schäfer, A. I. (2024). Differentiation of adsorption and degradation in steroid hormone micropollutants removal using electrochemical carbon nanotube membrane. *Nature Communications*, *15*, 9524.
52. Mane, P. V., Rego, R. M., Yap, P. L., Losic, D., & Kurkuri, M. D. (2024). Unveiling cutting-edge advances in high surface area porous materials for the efficient removal of toxic metal ions from water. *Progress in Materials Science*, *146*, 101314.
53. Mohamed, M. A., Jaafar, J., et al. (2017). Fourier Transform Infrared (FTIR) Spectroscopy. *Membrane Characterization*, *101*, 157–170. <https://doi.org/10.1016/B978-0-444-63776-5.00001-2>
54. Ji, Y., Yang, X., Ji, Z., Zhu, L., Ma, N., Chen, D., Jia, X., Tang, J., & Cao, Y. (2020). DFT-Calculated IR Spectrum Amide I, II, and III Band Contributions of N-Methylacetamide Fine Components. *ACS Omega*, *5*, 8572–8578. <https://doi.org/10.1021/acsomega.9b04421>
55. Movasaghi, Z., Rehman, S., & Rehman, I. U. (2008). Fourier transform infrared (FTIR) spectroscopy of biological tissues. *Applied Spectroscopy Reviews*, *43*, 134–179. <https://doi.org/10.1080/05704920701829043>
56. Hadjiivanov, K. I., Panayotov, D. A., Mihaylov, M. Y., Ivanova, E. Z., Chakarova, K. K., Andonova, S. M., & Drenchev, N. L. (2021). Power of Infrared and Raman Spectroscopies to Characterize Metal-Organic Frameworks and Investigate Their Interaction with Guest Molecules. *Chemical Reviews*, *121*, 1286–1424. <https://doi.org/10.1021/acs.chemrev.0c00487>
57. Wu, Q., Higler, R., Kodger, T. E., & Van Der Gucht, J. (2020). Particle Dynamics in Colloid-Polymer Mixtures with Different Polymer Architectures. *ACS Applied Materials & Interfaces*, *12*, 42041–42047. <https://doi.org/10.1021/acsami.0c07153>
58. Huang, J., Yang, H., Chen, M., Ji, T., Hou, Z., & Wu, M. (2017). An infrared spectroscopy study of PES PVP blend and PES-g-PVP copolymer. *Polymer Testing*, *59*, 212–219. <https://doi.org/10.1016/j.polymertesting.2017.02.005>
59. Beygmohammadi, F., NourizadehKazerouni, H., Jafarzadeh, Y., Hazrati, H., & Yegani, R. (2020). Preparation and characterization of PVDF/PVP-GO membranes to be used in MBR system. *Chemical Engineering Research and Design*, *154*, 232–240. <https://doi.org/10.1016/j.cherd.2019.12.016>
60. Mikolaszek, B., Jamróiewicz, M., Mojsiewicz-Pieńkowska, K., & Sznitowska, M. (2022). Microscopic and Spectroscopic Imaging and Thermal Analysis of Acrylates, Silicones and Active Pharmaceutical Ingredients in Adhesive Transdermal Patches. *Polymers (Basel)*, *14*, 2888. <https://doi.org/10.3390/polym14142888>
61. Menon, R. B., Lakshmi, V. S., Aiswarya, M. U., Keerthana, R., & Nair, S. C. (2018). Porphysomes-a paradigm shift in targeted drug delivery. *International Journal of Applied Pharmaceutics*, *10*, 1–6. <https://doi.org/10.22159/ijap.2018v10i2.23493>
62. Polyvinylpyrrolidone - PVP, Polyvidone, (n.d.). <https://www.sigmaaldrich.com/US/en/substance/polyvinylpyrrolidone123459003398> (accessed March 28, 2024).
63. Castro, J. I., Chaur, M. N., Llano, C. H. V., Valencia Zapata, M. E., Mina Hernandez, J. H., & Grande-Tovar, C. D. (2021). Biocompatibility study of electrospun nanocomposite membranes based on chitosan/polyvinyl alcohol/oxidized carbon nano-onions. *Molecules*, *26*, 4753. <https://doi.org/10.3390/molecules26164753>
64. Nurazzi, N. M., Asyraf, M. R. M., Rayung, M., Norraahim, M. N. F., Shazleen, S. S., Rani, M. S. A., Shafi, A. R., Aisyah, H. A., Radzi, M. H. M., Sabaruddin, F. A., Ilyas, R. A., Zainudin, E. S., & Abdan, K. (2021). Thermogravimetric analysis properties of cellulosic natural fiber polymer composites: A review on influence of chemical treatments. *Polymers (Basel)*, *13*, 2710. <https://doi.org/10.3390/polym13162710>
65. Chi, E. Y., Krishnan, S., Randolph, T. W., & Carpenter, J. F. (2003). Physical stability of proteins in aqueous solution: Mechanism and driving forces in nonnative protein aggregation. *Pharmaceutical Research*, *20*, 1325–1336. <https://doi.org/10.1023/A:1025771421906>
66. Rabeler, F., & Feyissa, A. H. (2018). Kinetic modeling of texture and color changes during thermal treatment of chicken breast meat. *Food Bioprocess Technol.*, *11*, 1495–1504. <https://doi.org/10.1007/s11947-018-2123-4>
67. Bhomia, R., Trivedi, V., Coleman, N. J., & Mitchell, J. C. (2016). The thermal and storage stability of bovine haemoglobin by ultraviolet-visible and circular dichroism spectroscopies. *Journal of Pharmaceutical Analysis*, *6*, 242–248. <https://doi.org/10.1016/j.jpha.2016.02.004>
68. Weiss, I. M., Muth, C., Drumm, R., & Kirchner, H. O. K. (2018). Thermal decomposition of the amino acids glycine, cysteine, aspartic acid, asparagine, glutamic acid, glutamine, arginine and histidine. *BMC Biophysics*, *11*, 1–15. <https://doi.org/10.1186/s13628-018-0042-4>
69. Erkoç, T., Sevgili, L. M., & Çavuş, S. (2022). Hydroxypropyl cellulose/Polyvinylpyrrolidone Matrix Tablets Containing Ibuprofen:

- Infiltration. *Erosion and Drug Release Characteristics*, *ChemistrySelect.*, 7, e202202180. <https://doi.org/10.1002/slct.202202180>
70. Loría-Bastarrachea, M. I., Herrera-Kao, W., Cauich-Rodríguez, J. V., Cervantes-Uc, J. M., Vázquez-Torres, H., & Ávila-Ortega, A. (2011). A TG/FTIR study on the thermal degradation of poly (vinyl pyrrolidone). *Journal of Thermal Analysis and Calorimetry.*, 104(2), 737–742.
71. Franco, P., & De Marco, I. (2020). The use of poly(N-vinyl pyrrolidone) in the delivery of drugs: A review. *Polymers (Basel).*, 12, 1114. <https://doi.org/10.3390/POLYM12051114>
72. Sarkar, S., Ramanathan, N., & Sundararajan, K. (2018). Effect of Methyl Substitution on the N-H···O Interaction in Complexes of Pyrrole with Water, Methanol, and Dimethyl Ether: Matrix Isolation Infrared Spectroscopy and ab Initio Computational Studies. *The Journal of Physical Chemistry A*, 122, 2445–2460. <https://doi.org/10.1021/acs.jpca.8b00023>
73. Chopra, N., Kaur, D., & Chopra, G. (2018). Nature and Hierarchy of Hydrogen-Bonding Interactions in Binary Complexes of Azoles with Water and Hydrogen Peroxide. *ACS Omega.*, 3, 12688–12702. <https://doi.org/10.1021/acsomega.8b01523>

Publisher's Note Springer Nature remains neutral with regard to jurisdictional claims in published maps and institutional affiliations.